THE ASTROPHYSICAL JOURNAL, 553:307–320, 2001 May 20
© 2001. The American Astronomical Society. All rights reserved. Printed in U.S.A.

OPTICAL SPECTROSCOPY OF THE X-RAY TRANSIENT XTE J1118+480 IN OUTBURST[1]

GUILLAUME DUBUS,[2] RITA S. J. KIM,[3] KRISTEN MENOU,[3,4] PAULA SZKODY,[5] AND DAVID V. BOWEN[3]
Received 2000 September 10; accepted 2001 January 4

ABSTRACT

We report on optical spectroscopic observations of the X-ray transient XTE J1118+480 covering the period from 2000 April 7 to July 4. The spectrum is characterized by weak, broad, double-peaked Balmer and He lines on top of a blue continuum of slope $p \approx \frac{1}{3}$, as expected for an optically thick accretion disk. The weak Bowen blend seen in our spectra may indicate a low metallicity for the source. The presence of a partial S-wave pattern in the He II λ4686 line appears consistent with the reported photometric period $P_{\rm orb} = 4.1$ hr for XTE J1118+480. By using a combination of Doppler mapping and various theoretical arguments, we constrain plausible orbital parameters for the system: a mass ratio $0.02 \lesssim q \lesssim 0.1$ and an inclination $i \gtrsim 70°$ for a neutron star primary or $30° \lesssim i \lesssim 50°$ for a black hole primary with a mass between 4 and 10 $M_\odot$. Ca II absorption features observed at very high resolution constrain the interstellar hydrogen absorption column log $[N_{\rm H\,I}({\rm cm}^{-2})] \approx 20.45 \pm 0.2$, and the identification of three absorbing clouds indicate a distance to the source $\lesssim 1$ kpc, assuming the line of sight to XTE J1118+480 has average high-latitude properties. These results are discussed in the context of previous multiwavelength observations of this unusual system.

Subject headings: accretion, accretion disks — binaries: close — X-rays: stars

1. INTRODUCTION

Soft X-ray transients (SXTs) are compact binary systems in which a low-mass secondary (either a main-sequence star or a subgiant) transfers mass via Roche lobe overflow onto a black hole (BH) or neutron star (NS) primary (see reviews by Tanaka & Lewin 1995; van Paradijs & McClintock 1995; and White, Nagase, & Parmar 1995). SXTs have highly variable luminosities. They spend most of their lifetime in a low-luminosity quiescent state but occasionally undergo dramatic outbursts during which both their optical and X-ray emission increase by several orders of magnitude (see, e.g., Tanaka & Shibazaki 1996; Chen, Shrader, & Livio 1997).

The X-ray emission during the outburst of an SXT is typically dominated by relatively soft thermal emission from the accretion disk surrounding the compact object, while the optical emission is usually interpreted as reprocessed X-rays from the disk and/or the companion star. The new source XTE J1118+480 belongs to the class of SXTs, but it also possesses some rather unusual characteristics.

XTE J1118+480 was discovered on 2000 March 29 with the *Rossi X-Ray Timing Explorer* (*RXTE*) All-Sky Monitor (ASM) as a brightening X-ray source. Pointed *RXTE* observations confirmed the presence of this high Galactic latitude source ($l = 157.°7$, $b = +62.°3$), with a rather hard power-law emission spectrum of photon index $\Gamma \simeq 1.8$ up to 30 keV. It was subject to rapid X-ray flares, but no pulsation was detected. Retrospective ASM analysis revealed that the source experienced another modest outburst in 2000 January (Remillard et al. 2000; see Fig. 1). BATSE observations showed that the source is visible up to 120 keV (Wilson & McCollough 2000), and a 6.2 mJy (at 15 GHz) variable radio counterpart was later discovered (Pooley & Waldram 2000; Dhawan et al. 2000).

The $V \sim 13$ optical counterpart of XTE J1118+480 was found to correspond to an 18.8 mag star in the USNO catalog by Uemura, Kato, & Yamaoka (2000c; see also Uemura et al. 2000a). A photometric modulation on a 4.1 hr period was observed by Cook et al. (2000) and was later confirmed as a plausible orbital period by Patterson et al. (2000) and Uemura et al. (2000a; see Stull, Ioannou, & Webb in Haswell, Hynes, & King 2000a for a discrepant claim at twice this value). The photometric modulation was later reported to be changing shape and period, possibly showing the development of superhumps in this source (Uemura et al. 2000b). If these are normal superhumps, then the orbital period would be smaller than the photometric superhump modulation by a few percent.

Garcia et al. (2000) reported the first optical spectroscopic results on XTE J1118+480. They found an optical spectrum typical of SXTs in outburst, with very broad Hα, Hβ, and He II lines (FWHM $\gtrsim 2000$ km s^{-1}). These observations also indicated the presence of absorption features and a very low interstellar absorption $[E(B-V) \lesssim 0.024]$ to the source. These authors suggested that the surprisingly low X-ray ($\sim$40 mCrab, 2–12 keV) to optical ($V \sim 13$) flux ratio of XTE J1118+480 could be due to a nearly edge-on viewing angle.

Additional X-ray observations revealed the presence of a strong quasi-periodic oscillation (QPO) at 0.085 Hz in the X-ray light curve of XTE J1118+480. The shape of the power density spectrum and the hard emission spectrum of XTE J1118+480 prompted Revnivtsev, Sunyaev, & Borozdin (2000) to propose that the source is a BH transient by analogy with other such systems. The QPO was confirmed by *ASCA* observations, which also suggest the presence of a soft component in the spectrum (below 2 keV), possibly due to emission from the accretion disk in the system (Yamaoka

[1] Based on observations obtained with the Apache Point Observatory 3.5 m telescope, which is owned and operated by the Astrophysical Research Consortium.

[2] Astronomical Institute "Anton Pannekoek," Universiteit van Amsterdam, Kruislaan 403, Amsterdam, SJ NL-1098, Netherlands; gd@astro.uva.nl.

[3] Princeton University, Department of Astrophysical Sciences, Peyton Hall, Princeton NJ 08544; rita@astro.princeton.edu, kristen@astro.princeton.edu, dvb@astro.princeton.edu.

[4] Chandra Fellow.

[5] Department of Astronomy, University of Washington, Physics/Astronomy Building, Stevens Way, Seattle, WA 98195; szkody@astro.washington.edu.

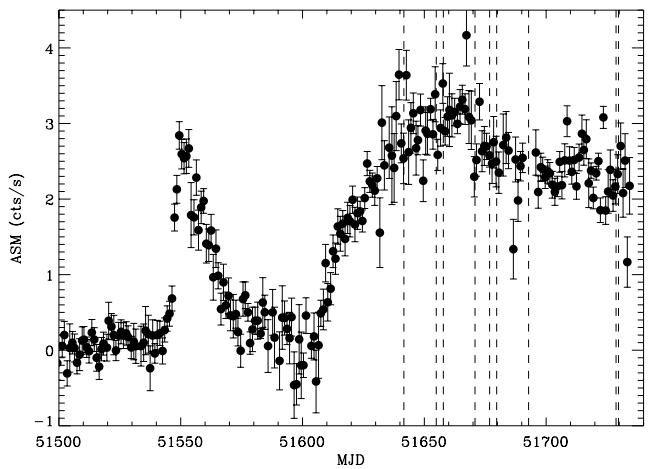

FIG. 1.—*RXTE* ASM light curve of XTE J1118+480, with dashed lines indicating the dates of our spectroscopic observations (see Table 1). Data provided by the ASM/*RXTE* teams at MIT and at the *RXTE* SOF and GOF at NASA's GSFC.

et al. 2000). Soft X-ray observations by *Chandra* did not confirm this (McClintock et al. 2001). The QPO frequency was reported to have shifted from 0.085 to $\gtrsim$0.1 Hz in subsequent observations (Wood et al. 2000; Yamaoka et al. 2000). Pointed *XTE* observations at the end of May do not reveal significant changes in the emission spectrum (P. Jonker 2000, private communication).

XTE J1118+480 has also been the subject of an extensive multiwavelength observation campaign with the *Hubble Space Telescope* (*HST*), *Extreme Ultraviolet Explorer* (*EUVE*), United Kingdom X-Ray Telescope (UKIRT), and *RXTE*. Thanks to the very low interstellar absorption to the source, the first *EUVE* spectrum of a BH candidate X-ray transient was obtained (Mauche et al. 2000). No periodic modulation was found in the *EUVE* data (Hynes et al. 2000b). An *HST* spectrum revealed a very broad (>10,000 km s^{-1}) Lyα absorption feature, suggestive of a massive accretor (Haswell et al. 2000a). Haswell et al. (2000b) obtained a near-UV power density spectrum of XTE J1118+480 with a QPO and an overall shape in agreement with previous *RXTE* timing data. In addition, the near-UV variability was found to lag by 1–2 s behind the X-ray variations, as would be expected from light echoes in a system with $P_{\rm orb} = 4.1$ hr. Hynes et al. (2000b), combining data from *HST*, *EUVE*, UKIRT, and *RXTE*, found that the IR to UV data suggests emission from both an optically thick disk and another flat-spectrum component (possibly synchrotron), while the *EUVE* and X-ray data suggest a power-law emission typical of a Galactic X-ray binary in a low/hard state. They conclude that XTE J1118+480, rather than experiencing a full outburst approaching the Eddington luminosity, seems to be in a minioutburst state (but see Kuulkers 2000).

In this paper, we describe the results of our optical spectroscopic campaign to monitor the evolution of XTE J1118+480 during its recent outburst (and early decline). In § 2, we describe our observations and the data reduction techniques used. Our results concerning the continuum and line emission, a partial S-wave pattern, and the interstellar absorption to the source are presented in § 3 and discussed in the context of the current knowledge of XTE J1118+480 in § 4. Our main conclusions are summarized in § 5.

2. OBSERVATIONS AND REDUCTION

We obtained optical spectra of XTE J1118+480 from 2000 April 7 to July 4 with the Astrophysical Research Consortium 3.5 m telescope at the Apache Point Observatory. We mostly used the Double Imaging Spectrograph (DIS), but spectra with the Echelle spectrograph were also obtained on 2000 April 7. Table 1 summarizes the dates and other characteristics of our observational campaign.

Most of our observations with DIS were carried out with the high-resolution gratings (hereafter HIRES) with a 1″.5 slit (dispersion 1.6 Å pixel^{-1} in the blue, 1.1 Å pixel^{-1} in the red, and a resolution of 2 pixels), but we also obtained spectra with the low-resolution gratings (same slit size, dispersion 6.2 Å pixel^{-1} in the blue, 7 Å pixel^{-1} in the red, and a resolution of 2 pixels; hereafter LOWRES) on 2000 April 7. For the DIS high-resolution observations, the blue and red gratings were centered on slightly different wavelengths during our various nights of observations, but we generally centered the blue side to cover the Hβ and He II λ4686 lines and the red side to cover the Hα line. The complete list of spectral coverage for our observations can be found in Table 1. The Echelle spectrograph covers the (fixed) wavelength range 3500–10,000 Å with $R \sim 30{,}000$ (10 km s^{-1} at 5000 Å) and a resolution element of $\sim$2.5 pixels. All the exposure times can be found in Table 1. The DIS observations were reduced in the standard way using *IRAF*, and the spectra were optimally extracted and dispersion corrected without any particular difficulty.

The Echelle spectra were reduced using the IRAF "ecspec" package. Direct extraction of the object spectra

TABLE 1

SPECTROSCOPIC OBSERVATIONS OF XTE J1118+480

Date (UT)	Epoch (HJD −2,400,000)	Instrument	Wavelength Coverage (Å)	Exposures (s)
2000 Apr 7	51,641.7	DIS LOWRES	4000–9000	2 × 60
		Echelle	3500–9800	2 × 600 + 12 × 1200
2000 Apr 20	51,654.9	DIS HIRES	4200–5000 / 5800–6800	26 × 300
2000 Apr 23	51,657.8	DIS HIRES	4200–5000 / 6200–7200	1 × 300
2000 May 6	51,670.8	DIS HIRES	4200–5000 / 6300–7300	1 × 480
2000 May 12.....	51,676.8	DIS HIRES	4200–5000 / 6300–7300	1 × 300
2000 May 15.....	51,679.7	DIS HIRES	4200–5000 / 6300–7300	1 × 300
2000 May 28.....	51,692.8	DIS HIRES	4200–5000 / 6300–7300	1 × 300
2000 Jul 3	51,728.7	DIS HIRES	4200–5000 / 6300–7300	1 × 300
2000 Jul 4	51,729.7	DIS HIRES	4350–5150 / 6050–7050	9 × 300 + 2 × 600

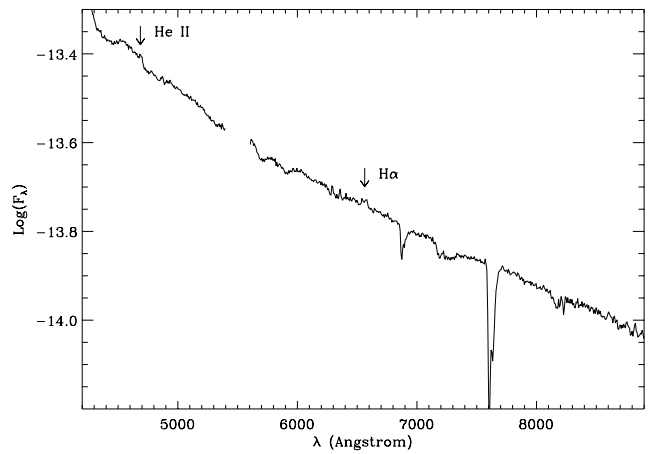

FIG. 2.—Representative spectrum of XTE J1118+480 obtained by summing the two DIS LOWRES spectra of 2000 April 7. The spectrum, typical of an X-ray transient in outburst, is characterized by a blue power-law continuum and the presence of relatively weak double-peaked emission lines, such as Hα and He II λ4686. The blank spectral region corresponds to wavelengths that are not efficiently covered by either the blue or the red side of the spectrograph. The unit for F_λ is ergs s^{-1} cm^{-2} Å^{-1}.

proved difficult for the highest (bluest) orders, where the trace was hard to follow. We decided to use the flat field as a guide and validated the method with a standard star observed on the same night. This resulted in significantly higher signal-to-noise ratios (S/Ns) in the blue part of the spectrum. A total of 115 orders were extracted covering the spectral range 3500–10,000 Å, in which the source is detected, albeit with varying sensitivity. The dispersion varied between ~0.05 and 0.1 Å pixel^{-1} and the usable spectral range in each order between ~70 and 150 Å from the blue to the red end, respectively.

The emission lines in the spectrum of XTE J1118+480 are both broad and weak (see below, Fig. 2), and their identification in the Echelle spectra turned out to be challenging. The broad lines can cover almost half of the spectral range in one order, making a continuum fit unreliable. We therefore proceeded by normalizing to an interpolated continuum determined from the two closest orders where no lines are expected. The normalized summed spectra clearly show Hα (in one order; left-hand panel of Fig. 3) and He II λ4686 (spread over two orders; right-hand panel of Fig. 3). These lines are also detectable in the individual continuum-subtracted Echelle spectra. The different profile of the He II line in the LOWRES and Echelle spectra is most probably due to the S-wave modulation discussed below. This S-wave is much less prominent in Hα.

3. RESULTS

The *RXTE* ASM light curve of XTE J1118+480 is shown in Figure 1 with the dates of our spectroscopic observations indicated by dashed lines. The source was in outburst during the entire period covered by our optical observations, with a flux of about 40 mCrab in the 2–12 keV band (Fig. 1). Optical photometry[6] also shows the source in outburst with a mean magnitude that decreased at most by 0.5 mag (from its peak value $\lesssim$13 mag) at the end of our observational program. Since then, the optical and X-ray fluxes have decreased significantly, indicating that the source may soon enter quiescence.

3.1. *Continuum*

Figure 2 shows the sum of the two DIS LOWRES spectra obtained on 2000 April 7, which are also representative of other spectra of the source obtained later during our campaign. The strong, blue power-law continuum and the weak emission lines are typical of an SXT in outburst (see also

[6] VSNET observations available at http://www.kusastro.kyoto-u.ac.jp/vsnet.

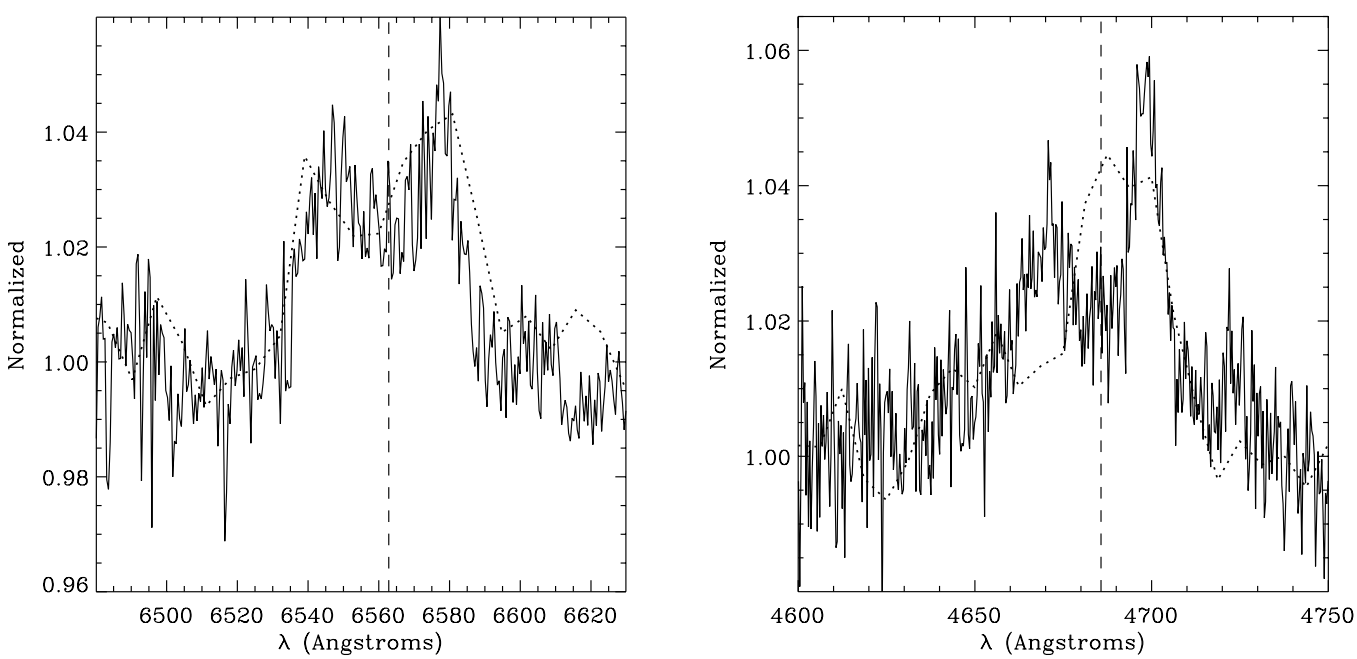

FIG. 3.—Hα (*left*) and He II (*right*) profiles for the summed Echelle spectra of April 7. Overplotted are the low-resolution spectra taken earlier on the same night. The Echelle spectra were also binned to 0.50 Å pixel^{-1} for Hα and 0.35 Å pixel^{-1} for He II.

Garcia et al. 2000). A power-law fit to the blue part of the spectrum yields a slope $p \simeq +0.4 \pm 0.2$ (where the flux $F_\nu \propto \nu^p$), while a similar fit to the red part of the spectrum yields $p \simeq +0.33 \pm 0.15$. These values are consistent with the expectation of $p = \frac{1}{3}$ for an optically thick accretion disk (see, e.g., Frank, King, & Raine 1992). Hynes et al. (2000b) find that the spectrum is flat using a wider wavelength range.

The broad, double-peaked Hα emission line is the only one easily identified on the spectrum of Figure 2, but a closer examination reveals the presence of He II λ4686 and additional Balmer and He lines in the other spectra that we collected (see § 3.2 below). We find only marginal evidence for continuum variability in XTE J1118+480, both during the same night and from night to night. The lack of obvious variability is consistent with the long-term variations in the optical Variable Star Network light curve (<0.5 mag), the short timescale (<10 s) of the large-amplitude (>0.3 mag) flickering, and the low amplitude (0.052 mag) of the 4 hr modulation (Patterson et al. 2000).

3.2. *Line Profiles and Their Evolution during Outburst*

We identify three Balmer lines, three He lines, and the Bowen blend in our set of spectra. These are Hγ λ4340.5, He I λ4471.5, the Bowen blend at $\sim$4638 Å, He II λ4686.7, Hβ λ4861.3, He I λ4921.9, Hα λ6562.8, and He I λ6678.1 The lines are weak, broad, and double-peaked. Hβ, Hγ, and also the weaker He I λ4471.5 have double-peaked emission clearly embedded in a large absorption trough. There is no clear evidence of such absorption around Hα.

Figure 3 shows the Hα and He II line profiles in the summed Echelle spectrum with the low-resolution spectrum taken on the same night overplotted. We find no evidence for structures at high spectral resolution in the lines except for an excess at rest wavelength that would not be expected in a pure double-peaked disk profile. This component also seems to be present in the high-resolution DIS spectra (see Fig. 4). The Bowen blend, which is very weak in the DIS HIRES spectra, was not detected on April 7 in either the DIS LOWRES or Echelle spectra.

Measuring the lines proved difficult, not because of a lack of counts in the spectra but because of their intrinsic broadness and weakness. As a rule, we performed two-component Gaussian fits to the emission lines. For Hγ and Hβ, the two emission components were subtracted to measure the equivalent width (EW) and FWHM of the absorption trough. The EW of the lines varies (with large associated errors) within a night, but we could find no periodic behavior linked to the photometric period. We also tried to estimate the semiamplitude velocity of the primary K_1 by fitting the wings of the He II line (expected to trace the motion of the compact star) and folding around the suspected $P_{\rm orb}$ of 0.17 day. This did not lead to any result, as could be expected from the usually low K_1 of SXTs ($K_1 \lesssim 50$ km s^{-1}).

The evolution of these lines during the 3 months of observations is shown in Figure 4, after the underlying continuum was normalized to unity. When available, multiple spectra were summed to increase the S/N of the spectra. A comparison between the most comprehensive data sets (April 17 and July 4), where measurement errors can be minimized, shows that the two strongest lines, Hα and He II, did not change significantly. We conclude that there do not seem to be any long-term variations. The average properties of the lines are summed up in Table 2 (the quoted errors are the rms of the measurements).

In all our spectra the blue side of the absorption troughs in Hγ and Hβ is less strong than the red side. The measured central wavelengths of the absorptions are redshifted compared to the rest wavelength (which could be an artifact of the method we used to remove the double peaked emission). Fitting a Gaussian to the red part of the absorption while ignoring (but not subtracting) the emission lines gave higher equivalent widths (2.4 Å for Hγ and 2.0 Å for Hβ) and better agreement with the rest wavelength (7 Å redshift for both instead of 15 Å). Similar absorption redshifts were reported by Callanan et al. (1995) for GRO J0422+32. A plausible explanation would be that the shifts are due to distorted line profiles. Such asymmetric lines are observed in dwarf novae when the disk becomes eccentric and the system shows superhumps (Warner 1995). There is evidence for such superhumps in XTE J1118+480 (see discussion in § 4.3).

3.3. *Constraint on the EUV Flux*

The He II emission may be used to obtain a crude estimate of the extreme ultraviolet (EUV) flux from the source (see, e.g., Patterson & Raymond 1985) if one assumes that the λ4686 line stems from the recombination of He I photoionized in the disk by photons with energies between 55 and 280 eV. On the other hand, the Doppler map discussed below in § 3.5 shows that most of the He II emission is localized and in all likelihood associated with stream-disk interaction. In this case the λ4686 line would be pumped by collisional excitation rather than photoionization. The following estimate therefore only yields an upper limit on the EUV flux. This is still of interest since the upper limit is independent of the column density to the source.

We derive from our observations $F_{\lambda 4686} \approx 7 \times 10^{-14}$ ergs s^{-1} cm^{-2} and, from the values given by Haswell et al. (2000a), $F_{\lambda 1640} \approx 7 \times 10^{-13}$ ergs s^{-1} cm^{-2}. This favors case B recombination, for which one would expect $F_{\lambda 1640}/F_{\lambda 4686} \sim 7$ (Seaton 1978). Therefore, the region is optically thick to the ionizing flux but thin to the line, and a fraction $\epsilon \approx 0.2$ of the photoionized He I recombinations leads to λ4686 emission (Hummer & Storey 1987).

Following previous applications to soft X-ray transients (Marsh, Robinson, & Wood 1994; Hynes et al. 1998), the EUV flux $F_{\rm EUV}$ and the He II line flux $F_{\lambda 4686}$ are related

TABLE 2

EMISSION LINES AND ABSORPTION TROUGHS IN XTE J1118+480

Line	λ_0 (Å)	$\lambda_{\rm obs} - \lambda_0$ (Å)	EW (Å)	FWHM (1000 km s^{-1})
Hγ	4340.5	-2 ± 4	-1.1 ± 0.4	2.1 ± 0.5
	4340.5	15 ± 5	1.8 ± 0.5	3.5 ± 0.5
He I	4471.5	1 ± 5	-0.3 ± 0.2	1.9 ± 0.6
	4471.5	4 ± 5	0.7 ± 0.4	4.0 ± 0.8
Bowen blend	4638	8 ± 10	-0.5 ± 0.3	2.0 ± 1.1
He II	4686.7	0 ± 3	-1.5 ± 0.4	2.3 ± 0.4
Hβ	4861.3	-1 ± 5	-1.0 ± 0.3	1.8 ± 0.3
	4861.3	13 ± 6	1.5 ± 0.5	3.1 ± 0.4
He I	4921.9	2 ± 5	-0.2 ± 0.2	1.4 ± 0.6
Hα	6562.8	0 ± 2	-1.9 ± 0.4	1.8 ± 0.4
He I	6678.1	-1 ± 5	-0.6 ± 0.4	1.8 ± 0.8

NOTE.—Negative equivalent widths indicate emission lines, while positive values correspond to absorption troughs. λ_0 is the rest wavelength and $\lambda_{\rm obs}$ is the central wavelength at which each feature is observed.

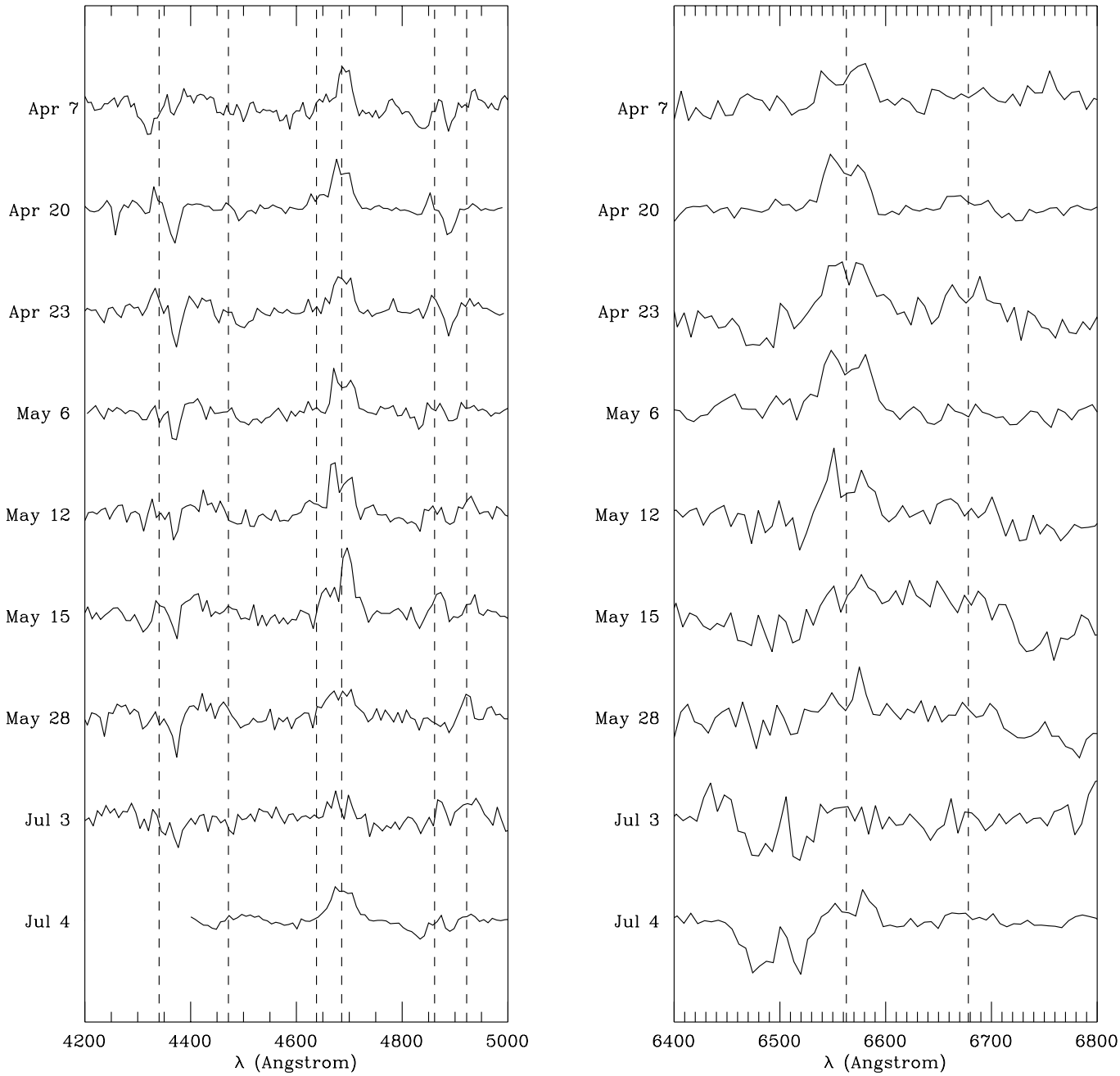

FIG. 4.—Evolution of the line profiles over the 3 month period of observation. The location of Hγ λ4340.5, He I λ4471.5, the Bowen blend at ∼4638 Å, He II λ4686.7, Hβ λ4861.3, He I λ4921.9, Hα λ6562.8, and He I λ6678.1 are indicated by vertical dashed lines. The spectra are the daily sums of the DIS HIRES spectra except for the top one, which is the sum of the two DIS LOWRES spectra obtained on 2000 April 7. The DIS HIRES spectra were further binned to reach a resolution comparable to that of the DIS LOWRES spectra. The vertical scale is identical for all spectra that were simply offset from each other. Note the two unidentified absorption features blueward of Hα.

through

$$\epsilon\alpha \frac{F_{\rm EUV}}{E_{\rm EUV}} = \frac{F_{\lambda 4686}}{E_{\lambda 4686}}, \quad (1)$$

where α is the fraction of EUV photons intercepted by the disc, while $E_{\rm EUV} \approx 100$ eV and $E_{\lambda 4686} \approx 2.6$ eV refer to the mean energy of the photons. We have assumed $L_{\rm EUV}/L_{\lambda 4686} = F_{\rm EUV}/F_{\lambda 4686}$, which may be incorrect if the EUV emission is not isotropic or if we see only a fraction of the He II emission. In both cases this assumption leads to an underestimate of the true EUV luminosity. Observations suggest that a fraction, $\sim 10^{-3}$, of the soft X-ray flux is intercepted and reprocessed in the optical by the accretion disk in SXTs (see, e.g., Dubus et al. 1999). By analogy, we take $\alpha = 10^{-3}$, from which we finally derive an upper limit to the 55–280 eV flux of 10^{-8} ergs s^{-1} cm^{-2}. This is obviously a very crude estimate.

An *EUVE* spectrum was obtained for this source, the first time ever for an SXT. The source flux at these wavelengths is heavily dependent on the extinction, but the upper limit on $F_{\rm EUV}$ derived above appears consistent with both a simple extrapolation of the optical-UV flux observed and the *EUVE* flux inferred if a value of $N_{\rm H} \approx 10^{20}$ cm^{-2} is assumed when dereddening the *EUVE* spectrum (Hynes et al. 2000b; Mauche et al. 2000).

3.4. *Peak-to-Peak Velocities*

The mean peak-to-peak separation for all the observations is 18 Å (1240 km s^{-1}) for Hγ, 23 Å (1470 km s^{-1}) for He II, 21 Å (1300 km s^{-1}) for Hβ, and 28 Å (1280 km s^{-1}) for Hα. The S-wave is much less prominent in the Balmer lines, and we assume that this represents the projected Keplerian velocity of the outer disk. The peak-to-peak separations have been found in well-known systems to overestimate the outer disk radius by about 20% because of sub-Keplerian motion or local broadening (Marsh 1998). This uncertainty is acceptable considering other assumptions made below. For a Keplerian disk with an emissivity $\propto R^{-n}$, Δv can be related to the outer (emitting) disk radius R_d by (Smak 1981)

$$\Delta v = 2R_d\Omega_{\rm K} \sin i = 2 \sin i(GM_1/R_d)^{1/2} , \qquad (2)$$

where M_1 is the mass of the primary and i the system inclination. We can also express R_d/a as a function of the velocity semiamplitude of the secondary K_2 and the mass ratio $q = M_2/M_1$ by combining the above equation with the mass function (see below and eq. [5]) and Kepler's third law,[7] resulting in

$$\frac{R_d}{a} = (1 + q)\left(\frac{2K_2}{\Delta v}\right)^2 . \qquad (3)$$

The disk outer radius is expected to reach the tidal truncation radius for $q \gtrsim 0.2$ and be limited to $R_d/a \approx 0.48$ by the 3:1 resonance for $q \lesssim 0.2$ (see, e.g., Warner 1995). Papaloizou & Pringle (1977, their Table 1) give a theoretical estimate of the outer disk radius, which we recklessly use for R_d/a. Equation (3) can therefore be used to give the semiamplitudes $K_2(q)$, for which the disk radius is consistent with the theoretical expectations. For $0.01 < q < 1$, the disk radius varies between 0.5 and 0.3 in units of the binary separation a. The expected K_2 as a function of q is shown as a solid line in the left-hand panel of Figure 8. We find 440 km s^{-1} $> K_2 >$ 260 km s^{-1} for $0.01 < q < 1$.

The observed velocity FWHM ($v_{\rm fwhm}$) of the lines provides an upper limit to the minimum emitting Keplerian disk radius:

$$R_{\rm in} \lesssim 1.3 \times 10^{10}(M_1/M_\odot)(\sin i/v_{\rm fwhm})^2 \text{ cm} , \qquad (4)$$

where $v_{\rm fwhm}$ is expressed in units of 1000 km s^{-1}. The absorption features from the optically thick disk (see § 4.1 and Table 2) have FWHM $\gtrsim$ 3000 km s^{-1}, implying $R_{\rm in} \lesssim 10^9$ cm. Haswell et al. (2000a) detect broad Lyα absorption with $v_{\rm fwhm} \sim 10^4$ km s^{-1}, which gives a stricter $R_{\rm in} \lesssim 10^8$ cm, or $R_{\rm in} \lesssim 500$ in Schwarzschild units. Spectral models of the X-ray low/hard state of BH candidates tend to predict larger values of $R_{\rm in}$ ($\gtrsim$1000 in Schwarzschild units) at which the transition from a thin disk to a hot advection-dominated flow occurs (see, e.g., Esin et al. 1998). The EUV flux of XTE J1118+480 could also imply a smaller transition radius (see § 4.2).

3.5. *Doppler Mapping*

Figure 5 shows the evolution of the He II λ4686 line profile over an approximately continuous 2.9 hr period on 2000 April 20. A partial S-wave pattern moves from the red to the blue side of the He II λ4686 line rest wavelength and appears consistent with the claimed photometric period of 4.1 hr (Cook et al. 2000; Patterson et al. 2000). The modulated component is particularly strong toward the middle of the observation at HJD 51,654.876, where it is blueshifted by about 900 km s^{-1}.

The trailed spectrum clearly shows that the Bowen blend, He I λ4921.9, Hγ, and Hβ follow the same S-wave pattern (see Fig. 5). We note that identical behavior is seen in the smaller continuous set (1.8 hr) of July 4, although with poorer S/N (not shown here). However, the presence of the S-wave in the Hα emission profile is not clear on either date.

Despite the incomplete phase coverage and the absence of a reference for superior conjunction of the secondary, we attempted to locate the emission site of the S-wave in the binary velocity plane using the Doppler tomography technique (Marsh & Horne 1988). Maps were reconstructed for He II and Hα for the April 20 observations using the software developed by Spruit (1998), assuming an orbital period of 0.1708 day and a null systemic velocity. It was not possible to combine this data set with our other observations since this would have required $P_{\rm orb}$ to be known much more accurately ($\Delta P_{\rm orb}/P_{\rm orb} = \Delta\phi P_{\rm orb}/T \sim 10^{-5}$ day with $T \approx 90$ days and an error on the phase set by the exposure time of $\Delta\phi = 0.01$). Furthermore, the 0.1708 day modulation is probably related to superhumps so that the orbital period can be expected to be close to this value with an uncertainty of a few percent. We tried several different orbital periods around 0.17 day, but this had no significant impact on the maps. The reconstructed trailed profiles and corresponding velocity maps are shown in Figures 6 and 7, respectively.

Each pixel on the projected Doppler map corresponds to an S-wave in the trailed spectra. The binary components are located on the y-axis of the map at positions corresponding to their semiamplitude velocities $(v_x, v_y) = (0, -K_1)$ for the primary and $(0, K_2)$ for the companion (indicated by crosses). However, since the orbital reference phase is arbitrary (here we chose $t_0 = 51{,}654.420$ in MJD), the map can be rotated in any fashion around the velocity origin. The secondary position, the ballistic gas stream trajectory, and the corresponding Keplerian velocity at the location of the stream shown on Figure 7 result from particular choices of K_2 and $q = M_2/M_1 = K_1/K_2$ discussed further below.

The trailed emission of He II shows a nice S-wave pattern that is consistent with the reported 0.1708 day photometric period (Cook et al. 2000; Patterson et al. 2000). Most of the He II emission originates from a localized region, but there is also an underlying (double-peaked) disk component that is visible in the original data. On the other hand, the disk dominates the Hα profile, producing a ring of emission in the velocity map. We also note the regions of enhanced Hα emission at about $(-910, 0)$ km s^{-1} (consistent with the He II S-wave) and $(-210, -730)$ km s^{-1}. The peak at the velocity origin (the center of mass) is due to the Hα emission component at rest wavelength discussed in § 3.2.

The bright emission region is typically associated with emission arising from the stream-disk interaction region or from the X-ray–heated surface of the secondary (see, e.g., Smak 1985; Marsh et al. 1994; Casares, Charles, & Marsh 1995a; Casares et al. 1995b; Harlaftis, Horne, & Filippenko 1996; Harlaftis, Charles, & Horne 1997a; Harlaftis et al. 1997b; Hynes et al. 2000a). Some SXTs also have low-

[7] From $P_{\rm orb} = 0.17$ day, Kepler's third law gives a binary separation $a \approx 10^{11}$ cm with a weak dependence on M_1 and q.

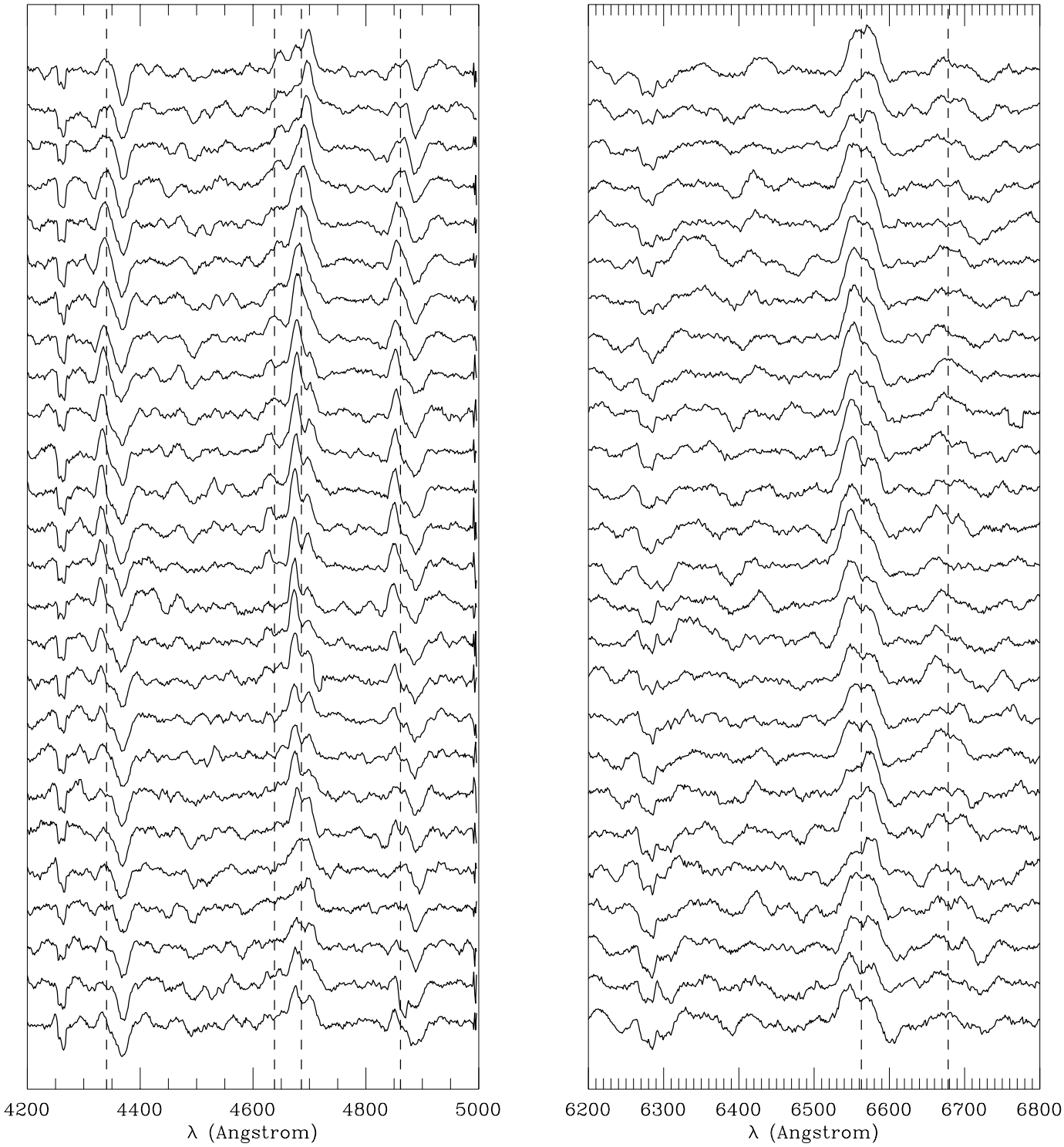

FIG. 5.—Time-resolved spectroscopy of XTE J1118+480 on 2000 April 20 reveals the presence of an S-wave pattern in the He II λ4686 emission as well as in the Bowen blend, Hβ, and Hγ (*dashed lines*). The S-wave is less prominent in Hα. The 26 spectra (which have been smoothed to enhance the features) have 5 minute exposures, and the set covers a total of 2.9 hr. The S-wave pattern, which is moving from the red to the blue side of the double-peaked line, is consistent with the claimed photometric orbital period of 4.1 hr.

velocity emission regions in their Doppler maps, possibly associated with a magnetic propeller (Hynes et al. 2000a). Here, the velocity of $\sim$900 km s^{-1} makes it doubtful that we observe such a phenomenon.

Assuming the He II emission arises from the heated hemisphere of the secondary, the semiamplitude 900 km s^{-1} (underestimating the real K_2) gives a rough constraint on the mass function through

$$f(M) = \frac{M_1^3 \sin^3 i}{(M_1 + M_2)^2} = \frac{K_2^3 P_{\rm orb}}{2\pi G} . \quad (5)$$

This gives a *minimum* mass for the primary of 12 $M_\odot$, which would make XTE J1118+480 at least as massive as the

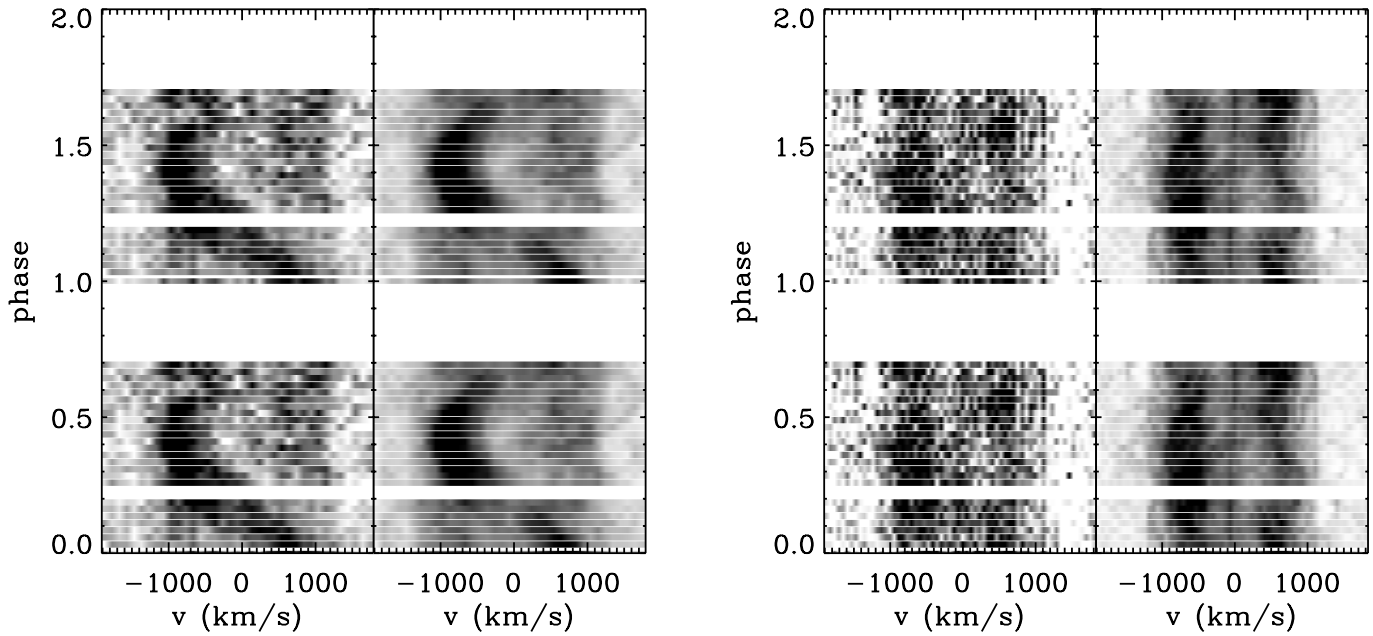

FIG. 6.—Observed (unsmoothed data) and reconstructed trailed emission line profiles on 2000 April 20 of He II λ4686 (*left*) and Hα (*right*). The corresponding Doppler maps are shown in Fig. 7. The assumed orbital period is 0.1708 day, the system has a null systemic velocity, and the orbital phase is arbitrary. The velocity reference is the rest wavelength of the emission line. Note the clear S-wave in the He II emission profile. The data are shown twice for clarity.

black hole in V404 Cyg. Lower inclinations would imply an even greater mass, making this system rather unusual compared to the dynamical masses inferred in other SXTs (see, e.g., van Paradijs & McClintock 1995). Although we cannot formally reject this possibility, the He II emission is unlikely to originate from the heated surface of the secondary.

The He II emission is more likely to originate from the stream-disk interaction. Typically, the hot spot is located (see above references) somewhere between the ballistic gas stream trajectory and its corresponding Keplerian velocity (which defines a circularization radius). We derive a lower limit on $K_2(q)$ (hence a lower limit on the primary mass) by assuming that the emission is located at the intersection of the two trajectories. The values of K_2 and q, for which the intersection matches the He II emission, are plotted as a dashed line in the left-hand panel of Figure 8.

A comparison between the two estimates of $K_2(q)$ shows that values of $0.02 \lesssim q \lesssim 0.1$ best fit the data, in the sense that they minimize the discrepancies. Formal agreement requires $q \approx 0.045$ ($K_2 \approx 430$ km s^{-1}), but this is, of course,

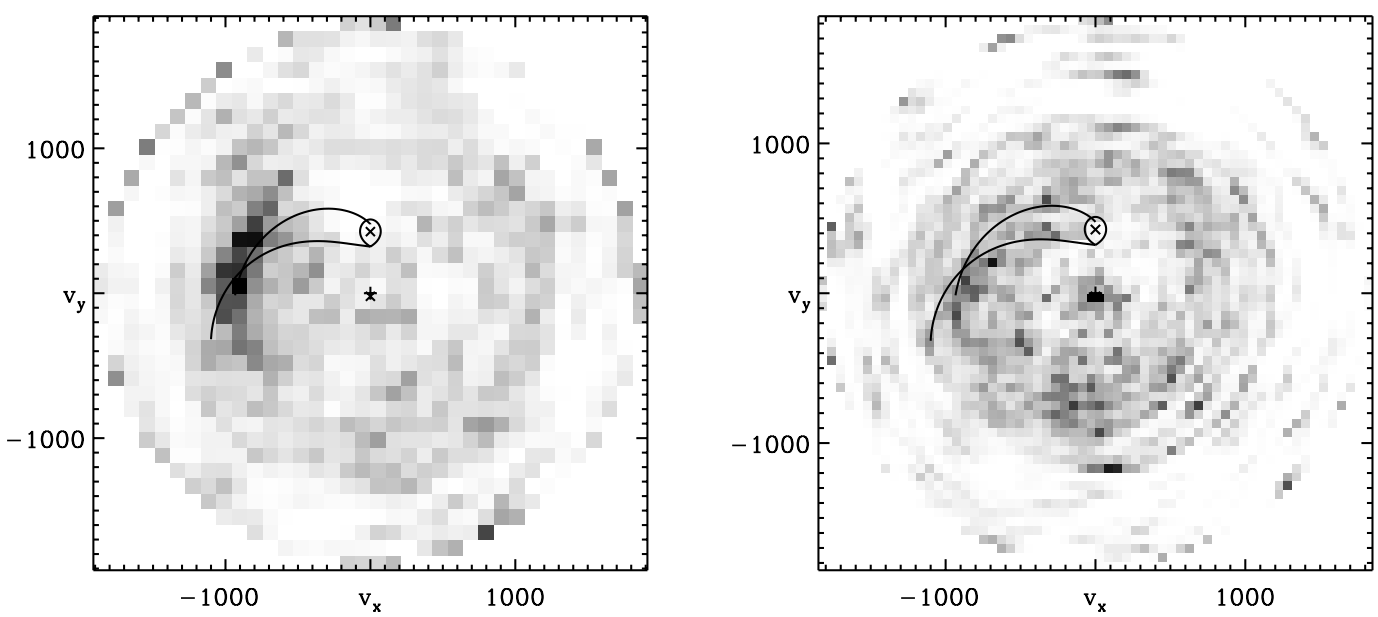

FIG. 7.—Reconstructed projected velocity maps (in km s^{-1}) for the He II (*left*) and Hα (*right*) emission during the April 20 observation (see Fig. 6). Also shown are the location of the binary components (*crosses*), the trajectory of the accretion stream from the secondary and corresponding Keplerian velocity for $q = 0.05$ and $K_2 = 420$ km s^{-1}. For this particular choice of parameters, and for an appropriate orbital reference phase, the emission region in the lower left-hand quadrant is associated with stream-disk interaction (the hot spot).

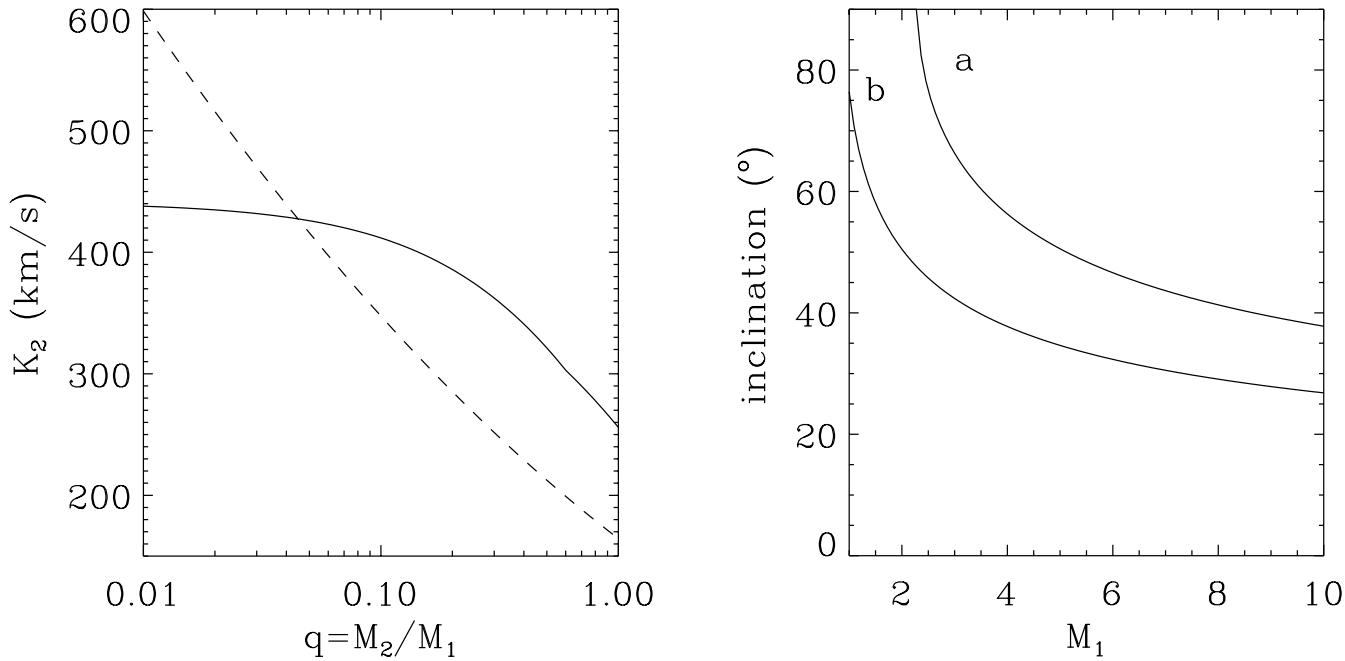

FIG. 8.—*Left*: Estimates of $K_2(q)$. The solid line was obtained by assuming that the peak-to-peak velocity of the Hα line represents the velocity of the outer radius R_d of a Keplerian disk, with $R_d(q)$ given by theoretical arguments on disk truncation. The dashed line was obtained by forcing the ballistic gas stream trajectory and its corresponding Keplerian velocity to intersect at the location of the He II emission region in the Doppler map (Fig. 7). Given the (large) uncertainties involved, we consider the agreement acceptable for $0.02 \lesssim q \lesssim 0.1$. *Right*: Estimate of the inclination i as a function of the primary mass M_1. Given K_2 and q, $i(M_1)$ is obtained from the mass function (eq. [5]). The two curves correspond to the extreme values of q and K_2 derived from the left-hand panel (*a* for $q = 0.02$ and $K_2 = 500$ km s^{-1}; *b* for $q = 0.1$ and $K_2 = 350$ km s^{-1}). Values in between the two curves are acceptable within our assumptions. The high inclinations required for small values of M_1 (in solar masses) are necessary to explain the high peak-to-peak velocity (hence outer disk velocity) in the data.

model dependent. Knowing q and K_2, the mass function (eq. [5]) gives the inclination i as a function of M_1. This relation is plotted in Figure 8 (right-hand panel) for the two extreme cases, $q = 0.02$ and $K_2 = 500$ km s^{-1} and $q = 0.1$ and $K_2 = 350$ km s^{-1}. Clearly, an NS would require large inclinations, while a BH gives intermediate inclinations. Given the assumptions made for the interpretation of the peak-to-peak velocity and the He II emission, we are likely to underestimate K_2 in both cases. This would only strengthen the case for a black hole primary.

The stream-disk interaction apparently extends some way along the Keplerian velocity trace as previously seen in other SXTs (see, e.g., Harlaftis et al. 1996). This could also be a numerical artifact, possibly due to an inaccurate orbital period. The second weaker emission region in the Hα velocity map could be due to continued disturbance of the accretion disk further along in azimuth. In this picture the stream-disk interaction takes place inside the disk, as emphasized by the larger velocity amplitude of the S-wave with respect to the peak-to-peak amplitude of the Balmer emission lines. This interpretation suggests significant stream overflow above the outer disk and an interaction region close to the circularization radius. Alternatively, systematic effects leading to lower observed peak-to-peak velocities (e.g., local line broadening; Marsh 1998) would place the hot spot closer to the disk outer edge.

3.6. *Interstellar Absorption*

The Echelle spectra of XTE J1118+480 obtained on 2000 April 7 reveal the presence of weak Ca II λ3933 absorption features, which can be used to estimate the neutral hydrogen absorption column to the source. The spectra also show Ca II λ3968 in absorption, with an equivalent width of an order one-half that of Ca II λ3933 features, as expected for this doublet (see, e.g., Cohen 1975). Both features are seen on two overlapping orders with similar structure. The Ca II lines are detected in some of the individual Echelle exposures with identical profiles. Figure 9 shows the Ca II λλ3933, 3968 absorption features in the summed Echelle spectra. The two orders have also been summed for this plot, with weighting corresponding to the different sensitivities at the locations of the Ca II lines.

A Gaussian fit to each of the three absorption components yields heliocentric velocities $v_0 \simeq -44$, -26, and -5 km s^{-1}. These velocities are consistent with an absorption component clearly seen at roughly -44 km s^{-1} and the hint of another component at -26 km s^{-1} in Na I λλ5889, 5895. The presence of strong Na emission at the rest wavelength (sky emission) precludes the detection of the presumed third absorption component at -5 km s^{-1} and the use of Na absorption for the determination of the H I absorption column, $N_{\rm H\,I}$, to XTE J1118+480.

We proceed as follows to determine $N_{\rm H\,I}$.[8] We assume that the gas in each absorbing cloud has a Maxwellian velocity distribution centered on its heliocentric velocity v_0, so that the Ca II optical depth of the cloud can be described by (Spitzer 1978)

$$\tau[v - v_0] = N_{\rm Ca\,II} \frac{\sqrt{\pi} e^2 f \lambda_0}{m_e c b} e^{-[(v - v_0)/b]^2} , \qquad (6)$$

[8] Note that we do not have to worry about a stellar Ca II absorption component from the companion star because the emission of XTE J1118+480 in outburst is presumably dominated by accretion.

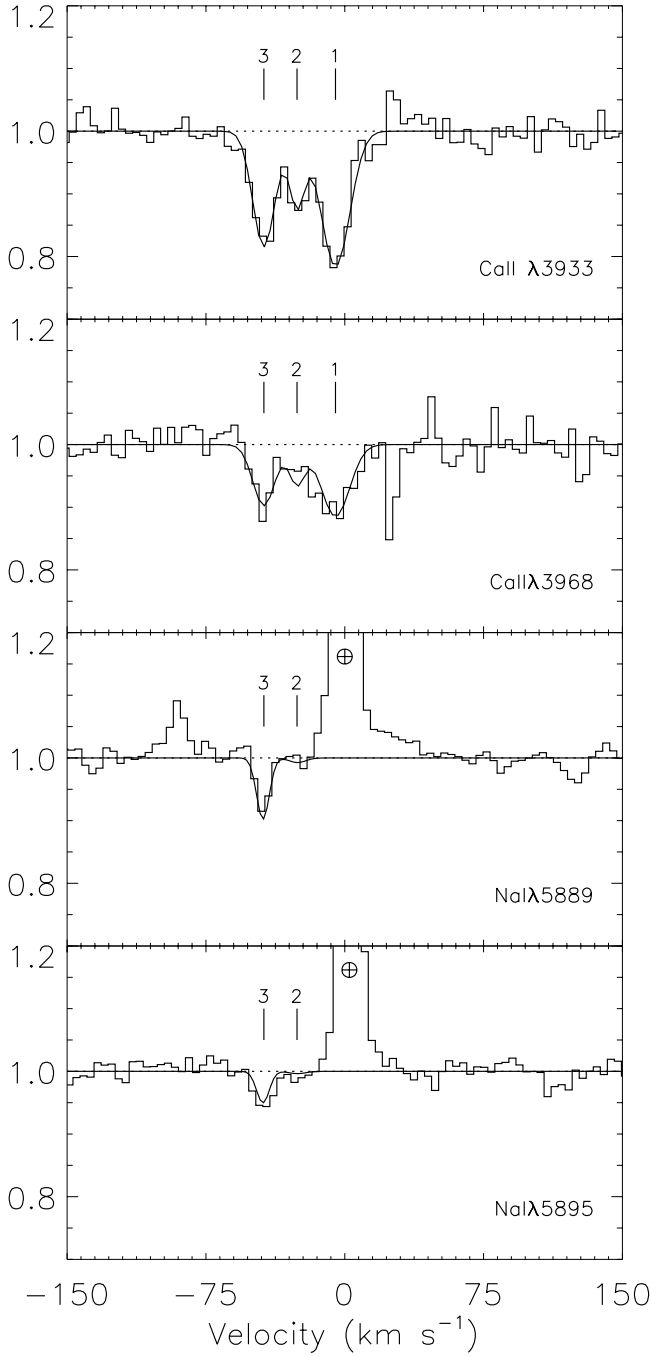

FIG. 9.—Echelle spectroscopy of XTE J1118+480 reveals three narrow interstellar Ca II λ3933.6 absorption lines (seen also in Ca II λ3968 and Na I λλ5889, 5895). The total equivalent widths are 0.108 ± 0.009 Å for the Ca II λ3933 lines and 0.061 ± 0.008 Å for the Ca II λ3968 lines. All the absorption features shown in the four panels above (summed Echelle spectra) are fully consistent with each other, in width and velocity (note the Na I sky emission at rest wavelength). In each panel, the data are shown as an histogram, the solid line shows a fit to the absorption lines, and the dotted line a fit to the continuum. The three Ca II lines can be used to constrain the low hydrogen absorption column and distance to the source (see text for details).

where $N_{\rm Ca\,II}$ is the total cloud absorption column, $\lambda_0 =$ 3933.6 Å is the rest wavelength of the Ca II K line, $f = 0.688$ is the oscillator strength of this transition (Cardelli & Wallerstein 1986), b is the velocity dispersion of the cloud, e is the charge of the electron, m_e is the mass of the electron, and c is the speed of light. Relative to a unity continuum, the line profile of a given absorbing cloud component has a depth given by

$$e^{-\tau[v-v_0]} \tag{7}$$

at any speed v (or, equivalently, wavelength) around the central value v_0.

To deduce precise values of b and $N_{\rm Ca\,II}$, we have compared the observed Ca II line profiles with theoretical, multicomponent absorption line profiles. Initial profiles were calculated using the values of b and $N_{\rm Ca\,II}$ derived from equations (6) and (7), which were then convolved with a Gaussian instrumental line spread function whose FHWM was measured from the arc lines used to wavelength calibrate the data. The best values of b and $N_{\rm Ca\,II}$ were found by minimizing χ^2 between the data and the theoretical fits. The resulting values for the Ca II lines are $b = 9.1$, 2.4, and 6.2 km s^{-1} and log $N_{\rm Ca\,II} = 11.85$, 11.34, and 11.67 for the components at $v_0 = -5$, -26, and -44 km s^{-1}, respectively.

The translation of the Ca II absorption column to an hydrogen absorption column is somewhat delicate, especially in view of the possibly efficient deposition of gaseous Ca II onto dust grains (see, e.g., Vallerga et al. 1993). However, there is a substantial body of observational data on Ca II absorption, which allows us to use an average value for the ratio $N_{\rm Ca\,II}/N_{\rm H\,I}$. In their independent studies, both Cohen (1975) and Sembach & Danks (1994) find an average value of log $[N_{\rm Ca\,II}/N_{\rm H\,I}] \simeq -8.3$ for high-latitude lines of sight, with approximate error bars of ± 0.2 in log in the two cases. Assuming this average is representative of the line of sight to XTE J1118+480, this translates into a value of log $[N_{\rm H\,I}({\rm cm}^{-2})] = 20.45 \pm 0.2$, where the error bars come from the conversion of Ca II to H I absorption.

We note that this estimate is somewhat larger than the values of log $[N_{\rm H\,I}({\rm cm}^{-2})] \approx 20$ considered as reasonable by Hynes et al. (2000b; see also Esin et al. 2001; McClintock et al. 2001) when dereddening the low-energy spectrum of XTE J1118+480. This discrepancy raises the possibility that the value obtained from the Ca II measurement overestimates the true value of $N_{\rm H\,I}$ on the line of sight to the source. Most likely, this would come from the conversion from Ca II to H I, which may not be "average" as assumed above for XTE J1118+480. It is also possible to measure the total $N_{\rm H\,I}$ along the sight line toward XTE J1118+480 from 21 cm emission observations. Using data from the Leiden/Dwingeloo Survey (Hartmann & Burton 1997), the H I column at $(l, b) = (157.5, 62.0)$ is 1.32×10^{20} cm^{-2}, a factor of 2 lower than we derive. This value represents an *upper* limit of course, since the 21 cm emission is integrated along the line of sight through the entire Milky Way. This therefore also suggests that our value of $N_{\rm H\,I}$ is overestimated, although the Dwingeloo beam size of 36′ is too large to measure higher $N_{\rm H\,I}$ over smaller angular scales, and it remains possible that a small, dense knot of H I with $N_{\rm H\,I} \gg 1.3 \times 10^{20}$ cm^{-2} could be lying directly along the line of sight.

It is encouraging to see that the properties derived above for the clouds are consistent with the average properties of high-latitude lines of sight described in Sembach & Danks (1994): $\langle N_{\rm Ca\,II}\rangle = (4.3 \pm 1.3) \times 10^{11}$ cm^{-2}. Furthermore, these authors find that, along extended sight lines at high latitude, the average number of absorbing Ca II clouds is 3.6 kpc^{-1}. This indicates that XTE J1118+480 is located at a distance ≈ 0.83 kpc if the line of sight to the source has

average properties, an estimate which is consistent with those for other SXTs. The actual distance to XTE J1118+480 could be somewhat different if this line of sight has properties deviating significantly from the mean. Note that our estimate of the distance is in rough agreement with that of Uemura et al. (2000a), who use the 18.8 quiescent magnitude to derive $d \sim 0.5$ kpc (M-type secondary) or $d \sim 1.5$ kpc (K-type secondary), and is consistent with the 0.8 kpc distance estimate of McClintock et al. (2001), assuming that the primary is a massive BH and that one-third of the light in quiescence is provided by the M dwarf secondary. It is also of interest to note that the 21 cm emission from the Leiden/Dwingeloo Survey mentioned above shows two peaks in brightness temperature, which correspond closely to the Ca II components at -5 and -44 km s^{-1}. Although the distance of the H I is not known, the scale height of H I in the Milky Way is ~ 1 kpc, and since the 21 cm emission arises from *all* the H I in the Galaxy along the sight line, XTE J1118+480 must be sufficiently far away so as to show the Ca II absorption from both H I components. This again suggests a significant distance between us and XTE J1118+480.

4. DISCUSSION

4.1. *The Absorption Troughs*

An interesting feature of the spectra is the absorption troughs in Hγ and Hβ. Although rarely discussed (see, however, Soria, Wu, & Hunstead 2000), these have been observed in several other transients with similar FWHM, including GRO J1655−40, A0620−00, GS 1124−68, Nova Mus 91, XTE J2123−058, XTE J1859+226, and especially GRO J0422+32, which bears many similarities to XTE J1118+480 (see § 5).

This type of line profile is also seen in dwarf novae (DNe) and nova-like (NL) systems, which are analogous to low-mass X-ray binaries (LMXBs), except for a primary that is a white dwarf. Typically, the spectrum of quiescent DNe display strong emission lines that are gradually replaced by absorption features during the rise to outburst and vice versa during the decay (see, e.g., Szkody, Piché, & Feinswog 1990).

Schematically, the absorption is thought to arise from the optically thick accretion disk, while the emission is thought to result from photoionization in a chromosphere-like, optically thin region above the disk. A key feature is that the expected spectrum is inclination-dependent since the absorption should disappear as the system gets closer to being edge-on because of strong line limb darkening in the two-dimensional disk (see, e.g., la Dous 1989; Marsh & Horne 1990; Wade & Hubeny 1998). There is indeed such an observed dependence in both DNe and NL systems, with the highest inclination systems showing only emission lines (la Dous 1991).

Although the detected absorption makes it unlikely that the inclination of XTE J1118+4800 is very high, this constraint is weak. For instance, GRO J1655−40 also showed Balmer absorption (Soria et al. 2000) but has a well-determined inclination of 70°. In contrast with DNe and NL systems, irradiation heating is much stronger in SXTs, where it usually dominates the heat balance in the outer disk regions (hence the optical emission; van Paradijs & McClintock 1994). Energy deposited by soft X-rays easily causes a thermal inversion in the top layers where the emission lines originate (see, e.g., Ko & Kallman 1994). If the optically thin atmospheres of SXTs are indeed more extended than in DNe, one would expect Balmer absorption not to be as common an occurrence as in the non-magnetic cataclysmic variables.

The spectral models of X-ray irradiated disks computed by Sakhibullin et al. (1998) show that softer irradiation leads to the disappearance of the absorption troughs. As the irradiation spectrum hardens, the X-ray photons deposit their energy in deeper disk layers, which do not contribute to the line emission. Inversely, any parameter change resulting in additional heating of the disk atmosphere leads to more emission. Any combination of a low-inclination, low–X-ray luminosity, hard X-ray spectrum or a low fraction of reprocessed X-ray photons in the disk could explain the absorption troughs.

Those SXTs in which Balmer absorption has been observed have probably been guilty of one or several of the above. Interestingly, in GRO J0422+32, the Hα and Hβ lines evolved from absorption to emission within 3 days during the rise to one of the minioutbursts (Callanan et al. 1995). Although the authors could not find any evidence for increased X-ray flux between 0.5 and 10 keV, the simultaneous rise in He II emission does suggest a larger flux of soft 0.05–0.3 keV photons, which would have a strong effect on the chromosphere. However, a hard X-ray upturn in GRO J1655−40 was accompanied by a dramatic increase of Hα emission but also by a *decrease* of the He II λ4686 flux (Shrader et al. 1996). It seems difficult to identify the dominant culprit, but we propose the low X-ray flux (see next section) and the hard X-ray spectrum of XTE J1118+480 as prime suspects responsible for the absorption troughs observed.

4.2. *The Optical Magnitude*

A unique characteristic of this system is the large optical to X-ray ratio compared to other SXTs. The ratio for XTE J1118+480 is not dissimilar (Garcia et al. 2000) to that found in accretion disk corona (ADC) sources, where the X-ray flux is partly hidden by the disk seen edge-on. Yet, XTE J1118+4800 has not shown any of the typical behavior associated with ADC sources, namely X-ray dips or eclipses. In addition, our crude "fitting" of the peak-to-peak velocity of the Balmer lines and of the velocity map rather hints at intermediate inclinations.

This high ratio might simply be due to the low absorption and proximity of the source. At the ~ 0.8 kpc distance implied by the Ca II absorption, the 2–10 keV X-ray flux ($\approx 8 \times 10^{-10}$ ergs s^{-1} cm^{-2}; Yamaoka et al. 2000) is such that $L_x \approx 6 \times 10^{34}$ ergs s^{-1}. By analogy with the low/hard state of Cyg X-1, Fender et al. (2001) find the broadband X-ray luminosity is $\sim 10^{36}$ ergs s^{-1} cm^{-2} at 1 kpc; i.e. this outburst was weak for an SXT.

We compare the X-ray flux and optical magnitude M_V by computing the quantity $\Sigma = (L_x/L_{Edd})^{1/2}(P_{orb}/1\ \mathrm{hr})^{2/3}$, where $L_{Edd} = 1.3 \times 10^{38}(M_1/M_\odot)$ ergs s^{-1} is the Eddington luminosity. With $P_{orb} = 0.1708$ day, we find $\log \Sigma \lesssim -1.2$ with $M_1 = 1\ M_\odot$, while $M_V \approx 3.5$ for $V = 13$ and $E(B-V) = 0$. Within the error bars, this is consistent with the correlation found for other SXTs between $\log \Sigma$ and M_V by van Paradijs & McClintock (1994). In other words, the optical flux of XTE J1118+480 is roughly in agreement with what would be expected if the disk is irradiation-dominated.

The agreement is less good for higher M_1, the optical flux being larger than expected from the correlation. The X-ray–heated companion could contribute to the optical as in, e.g., the persistent LMXB Cyg X-2. In this case we might expect the He II emission to originate from the X-ray–heated surface of the secondary. We have argued that this is unlikely. A better candidate for this extra optical emission is synchrotron emission (Hynes et al. 2000b) originating in a magnetic corona (Merloni, Di Matteo, & Fabian 2000),[9] an advection-dominated accretion flow (ADAF; Esin et al. 2001), and/or a jet (~equivalent to the first model with the base of the jet acting as the magnetic corona; Markoff, Falcke, & Fender 2001). XTE J1118+480 probably has a powerful compact jet, with emission extending at least to the near-infrared (Fender et al. 2001). Both ADAF and magnetic corona models can explain the high optical/X-ray ratio, but the EUV predictions may differ. The model presented by Merloni et al. (2000) has a large blackbody component peaking at $\nu \approx 10^{16.5}$ Hz due to hard X-ray reprocessing in the disk. The soft X-ray observations of *Chandra* do not seem to support this model (Esin et al. 2001; McClintock et al. 2001).

4.3. *Superhumps?*

The detection of superhumps (Uemura et al. 2000b) could add several constraints to the system parameters. According to current models, superhumps appear when the disk can reach the 3:1 resonance radius, requiring small mass ratio $q \lesssim 0.3$ (Warner 1995). In principle, the relative difference between the superhump period and the orbital period can give an even better constraint on q (see, e.g., O'Donoghue & Charles 1996). Such a small mass ratio is compatible with the constraint $0.02 \lesssim q \lesssim 0.1$ that we derived in § 3.5.

In DNe and NL systems, the origin of the optical variation could lie in the enhanced viscous dissipation modulated on the superhump period. However, these variations should be swamped in SXTs, where irradiation heating rather than viscous heating dominates the optical output. Haswell et al. (2001) recently argued that the small change in the accretion disk area on the superhump cycle, rather than the enhanced viscous dissipation, would give the desired effect for SXTs. The amplitude of the superhump would however decrease with larger inclinations.

The detection of superhumps in XTE J1118+4800, if confirmed, would therefore either mean the disk was not irradiation dominated (which is unlikely considering, e.g., the correlated X-ray/near-UV behavior reported by Haswell et al. 2000b) or that the inclination is low enough for the variations of the area of the disk to be observable.

4.4. *Is XTE J1118+480 a Halo Object ?*

The high Galactic latitude of XTE J1118+480 ($b = +62°$) is in sharp contrast with the latitudes of other LMXBs that cluster next to the Galactic plane. Whether or not XTE J1118+480 is a halo object obviously depends on its actual distance. At our inferred $d \sim 0.8$ kpc, XTE J1118+480 lies ~0.7 kpc above the Galactic plane.

[9] Note that the corona model of Merloni et al. (2000) may be challenged by the observations of Haswell et al. (2000b), which show that the near-UV variability lags behind the X-ray variability by 1–2 s.

The distribution of BH LMXBs around the Galactic plane has a dispersion of ~0.5 kpc. The larger dispersion of NS LMXBs (~1 kpc) is probably due to larger kick velocities at birth (White & van Paradijs 1996). Whether XTE J1118+480 has a BH or an NS primary, its height above the Galactic plane is not much larger than for other LMXBs. For instance, White & van Paradijs (1996) find $z \approx 0.9$ kpc for the BH Nova Oph 1977.

A low-metallicity environment would be supported by the low Bowen to He II flux ratio ≈0.3 (Table 2) that we find (Motch & Pakull 1989). But the detection of N and the nondetection of C and O lines in the UV spectra have been used to argue that the matter has been CNO processed in the companion (Haswell et al. 2000a) and that, from an evolutionary point of view, $M_1 < 3\ M_\odot$ is preferred to allow for an evolved secondary. Considering that XTE J1118+480 is not extremely far from the distribution of other LMXBs above the Galactic plane and that CNO processing might explain the low Bowen/He II flux ratio, we conclude that there is no compelling evidence for a halo origin of XTE J1118+480.

5. CONCLUSION

Let us first summarize the main conclusions of this work:

1. The optical spectrum of XTE J1118+480 in outburst shows several variable broad and weak emission lines superposed on an $F_\nu \propto \nu^{1/3}$ continuum typical of an optically thick accretion disk. The He II line shows a strong S-wave pattern that is consistent with the claimed 0.1708 day photometric period. We see no other obvious periodic or long-term behavior in the lines.

2. We find from the Ca II lines that the interstellar absorption to the source is low (log $[N_{\rm H\,I}({\rm cm}^{-2})] = 20.45 \pm 0.2$) and that the presence of three intervening clouds suggests a distance of ~0.8 kpc to the source. Since the low Bowen to He II ratio could indicate CNO-processed material (Haswell et al. 2000a) rather than an intrinsically low metallicity, we conclude there is no strong evidence to support a halo origin for XTE J1118+480.

3. We estimate an upper limit for the 0.05–0.3 keV source flux $\approx 10^{-8}$ ergs s^{-1} cm^{-2}. The dereddened *EUVE* spectrum (using a column absorption log $[N_{\rm H\,I}({\rm cm}^{-2})] \approx 20$; Hynes et al. 2000b; McClintock et al. 2001) appears compatible with this value. This suggests that a significant fraction of the source flux is emitted in the EUV/soft X-ray band. Given the very strong dependence of the slope of the dereddened *EUVE* spectrum on $N_{\rm H\,I}$, it may be difficult to accommodate a higher value for $N_{\rm H\,I}$ as derived from Ca II absorption in § 3.6.

4. The absorption in Hγ, Hβ, and the Balmer jump (Hynes et al. 2000b), originating from the optically thick disk, suggests that X-ray heating of the atmosphere is not as strong as in other SXTs, which may be consistent with the (very) low X-ray flux and hard X-ray spectrum. This also disfavors very high inclinations, for which limb darkening would remove the absorption features.

5. The Balmer lines have peak-to-peak velocities of ≈1250 km s^{-1}. Assuming that this corresponds to the Keplerian velocity of the outer disk, we use theoretical arguments on the disk size to estimate $K_2(q)$. We find 250 km s^{-1} $\lesssim K_2 \lesssim$ 450 km s^{-1} for $0.01 < q < 1$.

6. Using the reconstructed Doppler tomogram, we tentatively identify the He II S-wave with the stream-disk interaction. This gives us a second estimate of $K_2(q)$, which, combined with the first one, restricts possible values for q to $0.02 \lesssim q \lesssim 0.1$. This further implies that if the primary is an NS system, the system should have a high inclination ($i \gtrsim 70°$), while for a BH primary, an intermediate inclination is preferred ($30° \lesssim i \lesssim 50°$ for $10\,M_\odot \gtrsim M_1 \gtrsim 4\,M_\odot$).

Superhumps (Uemura et al. 2000b), if they require $q < 0.3$ and low to intermediate inclinations (Haswell et al. 2001), the absence of dips or eclipses in the X-ray light curve, the lack of high-frequency QPOs (Revnivtsev et al. 2000), and the broad Lyα line (Haswell et al. 2000a), favor an intermediate inclination system containing a BH. All of the arguments above are, however, rather uncertain and model-dependent. The assumptions made to interpret the peak-to-peak velocity and He II emission probably underestimate K_2. A larger K_2 would strengthen the case for a black hole primary.

We conclude by emphasizing the similarities between XTE J1118+480 and the black hole LMXB GRO J0422+32 in minioutburst: both have orbital periods of $\sim$4 hr, stayed in the low/hard X-ray state during outburst, had low X-ray luminosities, showed superhumps, and had identical optical spectra (including the absorption troughs). Scaling the $V = 19.5$ secondary of GRO J0422+32 from $d \approx 2.5$ kpc to the distance of XTE J1118+480 ($\approx$0.8 kpc) gives $V = 18.5$, consistent with the reported 18.8 quiescent magnitude. The system parameters for GRO J0422+32 (taken from Chen et al. 1997) are also within our allowed range for a coherent explanation of both the Balmer line peak-to-peak velocity and the location of the He II emission in XTE J1118+480. Quiescent studies, which can constrain the spectral type of the secondary and K_2, will shed more light on this interesting object.

The authors are grateful to Mike Garcia and Jeff McClintock for very useful discussions, to Todd Tripp for sharing his knowledge of the APO Echelle spectrograph, and to Rob Hynes for a very useful referee report. We are indebted to Ed Turner for granting us some of his Director's Discretionary Time at APO. Support for this work was provided by NASA through Chandra Postdoctoral Fellowship grant PF 9-10006 awarded by the Chandra X-ray Center, which is operated by the Smithsonian Astrophysical Observatory for NASA under contract NAS 8-39073. G. D. acknowledges support from the European Commission through the TMR network Accretion on to Black Holes, Compact Stars and Protostars (contract ERBFMRX CT 98-0195) and from the Leids Kerkhoven-Bosscha Fonds. R. S. J. K. acknowledges support from NSF grant AST 96-16901 and the Princeton University Research Board. P. S. acknowledges support from NASA grant NAG 5-7278.

REFERENCES

Callanan, P. J., et al. 1995, ApJ, 441, 786
Cardelli, J. A., & Wallerstein, G. 1986, ApJ, 302, 492
Casares, J., Charles, P. A., & Marsh, T. R. 1995a, MNRAS, 277, L45
Casares, J., Marsh, T. R., Charles, P. A., Martin, A. C., Harlaftis, E. T., Pavlenko, E. T., & Wagner, R. M. 1995b, MNRAS, 274, 565
Chen, W., Shrader, C. R., & Livio, M. 1997, ApJ, 491, 312
Cohen, J. G. 1975, ApJ, 197, 117
Cook, L., Patterson, J., Buczynski, D., & Fried, R. 2000, IAU Circ. 7397
Dhawan, V., Pooley, G. G., Ogley, R. N., & Mirabel, I. F. 2000, IAU Circ. 7395
Dubus, G., Lasota, J.-P., Hameury, J.-M., & Charles, P. A. 1999, MNRAS, 303, 139
Esin, A. A., McClintock, J. E., Drake, J. J., Garcia, M. R., Haswell, C. A., Hynes, R. I., & Muno, M. P. 2001, ApJ, in press (astro-ph/0103044)
Esin, A. A., Narayan, R., Cui, W., Grove, J. E., & Zhang, S.-N. 1998, ApJ, 505, 854
Fender, R. P., Hjellming, R. M., Tilanus, R. J., Pooley, G. G., Deane, J. R., Ogley, R. N., & Spencer, R. E. 2001, MNRAS, 322, L23
Frank, J., King, A. R., & Raine, D. J. 1992, Accretion Power in Astrophysics (2d ed.; Cambridge: Cambridge Univ. Press)
Garcia, M., Brown, W., Pahre, M., McClintock, J., Callanan, P., & Garnavich, P. 2000, IAU Circ. 7392
Harlaftis, E. T., Charles, P. A., & Horne, K. 1997a, MNRAS, 285, 673
Harlaftis, E. T., Horne, K., & Filippenko, A. V. 1996, PASP, 108, 762
Harlaftis, E. T., Steeghs, D., Horne, K., & Filippenko, A. V. 1997b, AJ, 114, 1170
Hartmann, D., & Burton, W. B. 1997, Atlas of Galactic Neutral Hydrogen (Cambridge: Cambridge Univ. Press)
Haswell, C. A., Hynes, R. I., & King, A. R. 2000a, IAU Circ. 7407
Haswell, C. A., King, A. R., Murray, J. R., & Charles, P. A. 2001, MNRAS, 321, 475
Haswell, C. A., Skillman, D., Patterson, J., Hynes, R. I., & Cui, W. 2000b, IAU Circ. 7427
Hummer, D. G., & Storey, P. G. 1987, MNRAS, 224, 801
Hynes, R. I., Charles, P. A., Haswell, C. A., Casares, J., & Zurita, C. 2000a, in Proceedings of Astro-Tomography Workshop, ed. H. Boffin & D. Steeghs (Berlin: Springer)
Hynes, et al. 1998, MNRAS, 300, 64
Hynes, R. I., Mauche, C. W., Haswell, C. A., Shrader, C. R., Cui, W., & Chaty, S. 2000b, ApJ, 539, L37
Ko, Y.-K., & Kallman, T. R. 1994, ApJ, 431, 273
Kuulkers, E. 2000, A&A, Astron. Nachr., in press (astro-ph/0102066)
la Dous, C. 1989, A&A, 211, 131
———. 1991, A&A, 252, 100
Markoff, S., Falcke, H., & Fender, R. P. 2001, A&A, in press
Marsh T. R. 1998, in ASP Conf. Series 137, Wild Stars In The Old West: Proceedings of the 13th North American Workshop on CVs and Related Objects, ed. S. Howell, E. Kuulkers, & C. Woodward (San Francisco: ASP), 236
Marsh, T. R., & Horne, K. 1988, MNRAS, 235, 269
———. 1990, ApJ, 349, 593
Marsh, T. R., Robinson, E. L., & Wood, J. H. 1994, MNRAS, 266, 137
Mauche, C., Hynes, R., Charles, P., & Haswell, C. 2000, IAU Circ. 7401
McClintock, J. E., et al. 2001, ApJ, in press (astro-ph/0103051)
Merloni, A., Di Matteo, T., & Fabian, A. C. 2000, MNRAS, 318, L15
Motch, C., & Pakull, M. W. 1989, A&A, 214, L1
O'Donoghue, D., & Charles, P. A. 1996, MNRAS, 282, 191
Papaloizou, J. C. B., & Pringle, J. E. 1977, MNRAS, 181, 441
Patterson, J., et al. 2000, IAU Circ. 7412
Patterson, J., & Raymond, J. C. 1985, ApJ, 292, 550
Pooley, G. G., & Waldram, E. M. 2000, IAU Circ. 7390
Remillard, R., Morgan, E., Smith, D., & Smith, E. 2000, IAU Circ. 7389
Revnivtsev, M., Sunyaev, R., & Borozdin, K. 2000, A&A, 361, L37
Sakhibullin, N. A., Suleimanov, V. F., Shimanskii, V. V., & Suleimanova, S. L. 1998, Astron. Lett., 24, 22
Seaton, M. J. 1978, MNRAS, 185, 5P
Sembachs, K. R., & Danks, A. C. 1994, A&A, 289, 539
Shrader, C. R., Wagner, R. M., Hjellming, R. M., & Starrfield, S. G. 1996, A&AS, 120, 261
Smak, J. 1981, Acta Astron., 31, 395
———. 1985, Acta Astron., 35, 351
Soria, R., Wu, K., & Hunstead, R. W. 2000, ApJ, 539, 445
Spitzer, L. 1978, Physical Processes in the Interstellar Medium (New York: Wiley)
Spruit, H. C. 1998, unpublished (astro-ph/9806141)
Szkody, P., Piché, F., & Feinswog, L. 1990, ApJS, 73, 441
Tanaka, Y., & Lewin W. H. G. 1995, in X-ray Binaries, ed. W. H. G. Lewin, J. van Paradijs, & E. P. J. van den Heuvel (Cambridge: Cambridge Univ. Press), 126
Tanaka, Y., & Shibazaki, N. 1996, ARA&A, 34, 607
Uemura, M., et al. 2000a, IAU Circ. 7418
———. 2000b, PASJ, 52, L15
Uemura, M., Kato, T., & Yamaoka, H. 2000c, IAU Circ. 7390
Vallerga, J. V., Vedder, P. W., Craig, N., & Welsh, B. Y. 1993, ApJ, 411, 729
van Paradijs, J., & McClintock, J. E. 1994, A&A, 290, 133
———. 1995, in X-ray Binaries, ed. W. H. G. Lewin, J. van Paradijs, & E. P. J. van den Heuvel (Cambridge: Cambridge Univ. Press), 58
Wade, R. A., & Hubeny, I. 1998, ApJ, 509, 350
Warner, B. 1995, Cataclysmic Variables (Cambridge: Cambridge Univ. Press)

White, N. E., Nagase, F., & Parmar, A. N. 1995, in X-ray Binaries, ed. W. H. G. Lewin, J. van Paradijs, & E. P. J. van den Heuvel (Cambridge: Cambridge Univ. Press), 1
White, N. E., & van Paradijs, J. 1996, ApJ, 473, L25
Wilson, C. A., & McCollough, M. L. 2000, IAU Circ. 7390
Wood, K. S. et al. 2000, ApJ, 544, L45
Yamaoka, K., Ueda, Y., Dotani, T., Durouchoux, P., & Rodriguez, J. 2000, IAU Circ. 7427